

# Updated Determination of Ellis-Jaffe Sum Rules and Extraction of Quark Spin Content

Hua Zhou<sup>1,\*</sup>, Qing Yu<sup>1,†</sup> and Xing-Gang Wu<sup>2,‡</sup>

<sup>1</sup> School of Science, Southwest University of Science and Technology, Mianyang 621010, P.R. China

<sup>2</sup> Department of Physics, Chongqing Key Laboratory for Strongly Coupled Physics, Chongqing University, Chongqing 401331, P.R. China

(Dated: October 10, 2024)

In this paper, we explore the properties of the Ellis-Jaffe Sum Rule (EJSR) in detail, employing the Principle of Maximum Conformality (PMC) approach to address its perturbative QCD contribution including next-to-next-to-next-to-leading order (N<sup>3</sup>LO) QCD corrections. Using the PMC, we attain a precise perturbative QCD approximate for the EJSR, without the conventional ambiguity associated with the renormalization scale. Given the presence of the  $\alpha_s$  Landau pole near the asymptotic scale, we also utilize the low-energy  $\alpha_s$  model based on the analytic perturbative theory (APT) to recalibrate the EJSR behavior in the infrared region. By combining the PMC approach with the low-energy APT model, we achieved theoretical predictions of EJSR that align well with the experiments. Using deep learning, we also fit the contribution of the quark spin to the nucleon spin  $\Delta\Sigma$  and ultimately obtain  $\Delta\Sigma \approx 0.23^{+0.02}_{-0.06}$ , consistent with global fit results  $\Delta\Sigma = 0.24 \pm 0.07$ .

## I. INTRODUCTION

The high-luminosity, precision collider will yield a wealth of high-precision experimental measurements about nucleon structure functions. This will further reveal the dynamic laws of strong interaction [1–5]. Moreover, these experimental advancements have also inspired numerous efforts on the theoretical to probe the structure functions and their first moment, i.e. the Ellis-Jaffe Sum Rule (EJSR) [6]. As a pivotal sum rule in particle physics, the EJSR provides a framework for elucidating the intricate spin structure in protons and neutrons, encompassing the complicated interplay of contributions from quarks and gluons, offering invaluable insights into their fundamental properties. A detailed examination of EJSR will enhance our comprehension of the fundamentals of strong interaction and Quantum Chromodynamics (QCD). Additionally, the EJSR has been utilized to explore the hypothesis that strange quarks contribute minimally to the spin structure of nucleon [7]. The precise determination of the EJSR can also aid us in verifying the exact value of the Bjorken Sum Rule (BSR)  $\Gamma_1^{p-n}(Q) = \int_0^1 dx [g_1^p(x, Q^2) - g_1^n(x, Q^2)]$  [8–14], thereby extracting the accurate value of the strong coupling constant  $\alpha_s$ .

Under the  $\overline{\text{MS}}$  scheme, the EJSR can be expressed as

$$\begin{aligned} M_1(Q, \mu_r) &= \int_0^1 dx g_1^{p(n)}(x, Q) \\ &= \frac{1}{36} C^{ms}(Q, \mu_r) (\pm 3g_A + a_8) \\ &\quad + \frac{1}{9} C^s(Q, \mu_r) a_0(Q). \end{aligned} \quad (1)$$

where  $g_1^{p(n)}(x, Q)$  represents the spin-dependent structure function of proton or neutron, incorporating the Bjorken scaling variable  $x$ .  $\mu_r$  stands for the renormalization scale.  $g_A$  represents the axial vector coupling constant, and the plus and minus in front of  $g_A$  correspond to protons or neutrons, respectively.  $a_8$  is the isovector and flavor-octet axial charges of the nucleon [4] and  $a_0(Q)$  is the flavor-singlet axial charge. Since the non-singlet axial current is conserved in the massless quark limit, this implies that the elements  $g_A$  and  $a_8$  are renormalization group invariant. The  $C^{ms}$  and  $C^s$  respectively correspond to the non-singlet and singlet coefficient functions, both of which exhibit a dependency on the renormalization scale.

The three-loop calculations for  $C^{ms}$  and  $C^s$  have been completed in Refs.[15, 16]. However, the theoretical prediction of the EJSR still struggles to meet the expected accuracy standards, and there is a significant deviation from the experimental measurements. Substantial exploration and attempts have been undertaken to enhance the precision of the theoretical prediction of the EJSR, such as the MSR scheme [17], which aims to optimize the coefficient convergence of the perturbative expansion of the EJSR. In addition, the EJSR results also reveal significant renormalization scale uncertainty, which undoubtedly presents a challenge on our path toward achieving higher precision.

In conventional perturbation calculations, it is customary to set the renormalization scale  $\mu_r = Q$  to eliminate large logarithmic terms  $\log(\mu_r^2/Q^2)$  [18, 19]. Subsequently, the renormalization scale is varied within a specified range to evaluate the uncertainty that stems from it. However, this straightforward approach fails to satisfy the requirement of renormalization group invariance (RGI) and causes ambiguities in the renormalization scale and scheme [20–22]. According to the RGI, physical quantities should remain invariant, irrespective of the choice of renormalization scheme and scale. To be precise, if computations are carried out to a sufficiently

\*Electronic address: [zhouhua@swust.edu.cn](mailto:zhouhua@swust.edu.cn)

†Electronic address: [yuq@swust.edu.cn](mailto:yuq@swust.edu.cn)

‡Electronic address: [wuxg@cqu.edu.cn](mailto:wuxg@cqu.edu.cn)

high order, the RGI will automatically be satisfied due to the mutual cancellation of the perturbative expansion dependence on the renormalization scheme and scale at each order. However, when dealing with finite orders, the dependence of the renormalization scale and scheme cannot be fully canceled out. Furthermore, under an arbitrary choice of renormalization scale, mismatches between the strong coupling constant at each order and its corresponding perturbative coefficient may occur, leading to uncertainties in both the renormalization scale and scheme [18, 19, 23].

To put it differently, perturbative expansions at fixed order inherently contain uncertainties associated with the scheme and scale. An ill-suited scale selection will greatly reduce the accuracy of theoretical prediction, ultimately leading to substantial discrepancies between theoretical predictions and experimental results. Owing to the intricate nature of Feynman diagram calculations, only relatively low-order computations can currently be achieved. As a result, procuring a theoretical prediction for the EJSR that remains independent of the renormalization scale at finite orders is important for shedding light on nucleon structure functions. In this paper, we utilize the Principle of Maximum Conformality (PMC) approach to obtain a theoretical prediction of the EJSR that is independent of the renormalization scale.

The running behavior of  $\alpha_s$  is controlled by the renormalization group equation (RGE),

$$\frac{d\alpha_s(\mu_r^2)}{d\ln\mu_r^2} = \beta(\alpha_s) = -\sum_{i=0}^{\infty} \beta_i \alpha_s^{i+2}(\mu_r^2), \quad (2)$$

where the  $\beta_i$  functions have been computed up to the 5-loop under the modified minimal-subtraction ( $\overline{\text{MS}}$ ) scheme [24–28]. The terms  $\beta_i$  that appear in the series of Perturbative Quantum Chromodynamics (pQCD) can be reabsorbed into  $\alpha_s$ , thus facilitating an accurate determination of the true value of  $\alpha_s$ . Based on this foundation, the PMC is a systematic approach to eliminate the ambiguity inherent in the renormalization scheme and scale [29–35]. To be specific, the PMC determines a global effective coupling  $\alpha_s(Q_*)$  [36] (where  $Q_*$  represents the PMC scale, which serves as a proxy for the effective momentum flow within the process.) by utilizing the non-conformal  $\beta_i$  terms. Simultaneously, by absorbing all the non-conformal terms in the perturbative expressions, the PMC prediction is also independent of the choice of renormalization scheme [37], and meets the basic requirement of RGI of physical observations [22, 38, 39].

In this paper, we aim to employ the PMC single scale-setting approach to attain a renormalization scale-invariant prediction within pQCD for the EJSR and improve its theoretical prediction accuracy. Under the  $\overline{\text{MS}}$  scheme, the renormalized EJSR up to next-to-next-to-next-to-leading order (N<sup>3</sup>LO) can be expressed in the expansion of the strong coupling constant  $\alpha_s$ ,

$$M_1(Q, \mu_r) = \sum_{i=0}^3 M^{(i)}(Q, \mu_r) a_s^i(\mu_r), \quad (3)$$

where  $a_s(\mu_r) = \alpha_s(\mu_r)/\pi$ . The theoretical calculation of the EJSR has been calculated up to N<sup>3</sup>LO [15, 16]. However, the dependence on the renormalization scale begins at the NNLO, still leading to considerable overall theoretical uncertainties. To address this, the PMC approach is adopted in this paper to eliminate the uncertainties stemming from the renormalization scale, thereby enabling highly precise predictions for EJSR at the fixed order.

## II. CALCULATION TECHNOLOGY

Based on the degenerate relationship [40], the EJSR can be rewritten in the following perturbative form:

$$M_1(Q, \mu_r) = r_{0,0} + r_{1,0} a_s(\mu_r) + (r_{2,0} + \beta_0 r_{2,1}) a_s^2(\mu_r) + (r_{3,0} + 2\beta_0 r_{3,1} + \beta_0^2 r_{3,2} + \beta_1 r_{2,1}) a_s^3(\mu_r) \quad (4)$$

where the coefficients of  $r_{i,j}$  can be found in Refs.[16, 41, 42]. The scale-invariant conformal coefficients are represented by  $r_{i,0}$ , and the non-conformal coefficients are denoted as  $r_{i,j}$  ( $j \neq 0$ ):

$$r_{i,j} = \sum_{k=0}^j C_j^k \ln(\mu_r^2/Q^2) \hat{r}_{i-k,j-k}, \quad (5)$$

where  $\hat{r}_{i,j} = r_{i,j}|_{\mu_r=Q}$  and  $C_j^k = j!/k!(j-k)!$ . After applying the standard PMC procedure, all non-conformal  $\beta_i$ -terms can be absorbed into  $\alpha_s$ , resulting in a conformal series that is both renormalization scale and renormalization scheme independent, e.g.,

$$M_1(Q, \mu_r) = \hat{r}_{0,0} + \hat{r}_{1,0} a_s(Q_*) + \hat{r}_{2,0} a_s^2(Q_*) + \hat{r}_{3,0} a_s^3(Q_*). \quad (6)$$

Consequently, the EJSR escapes the ambiguity associated with the renormalization scale  $\mu_r$  and enhances its precision. Leveraging the known perturbation series, the PMC scale can be determined at the next-leading log (NLL) accuracy:

$$\ln \frac{Q_*^2}{Q^2} = T_0 + T_1 a_s(Q^2), \quad (7)$$

where

$$T_0 = -\frac{\hat{r}_{2,1}}{r_{1,0}}, \quad (8)$$

$$T_1 = \frac{2(\hat{r}_{2,0}\hat{r}_{2,1} - \hat{r}_{1,0}\hat{r}_{3,1})}{\hat{r}_{1,0}} + \frac{\hat{r}_{2,1}^2 - \hat{r}_{1,0}\hat{r}_{3,2}}{\hat{r}_{1,0}} \beta_0. \quad (9)$$

Notably,  $Q_*$  remains uninfluenced by any selection of the renormalization scale  $\mu_r$ . Thus, the ambiguity associated with the renormalization scale is effectively eliminated.

## III. NUMERICAL RESULTS AND DISCUSSIONS

For numerical calculation, we use  $g_A = 1.2723 \pm 0.0023$  [43] and  $a_8 = 0.58 \pm 0.03$  [4]. To facilitate ease of understanding and manipulation, we defined  $a_0(Q)$  in a proper

invariant way as a constant, e.g.,  $a_0 = 0.141$  at  $Q = 5$  GeV for further discussion [17].

#### A. Running behavior of the strong coupling constant $\alpha_s$

Based on Eq.(7), we can derive the evolution relationship between the  $Q_*$  and  $Q$ , as shown in Fig.1. It can be observed in Fig.1 that when  $Q$  is small, the effective momentum flow  $Q_*$  approaches the asymptotic scale  $\Lambda_{\text{QCD}}$ . The strong coupling constant  $\alpha_s$  has an unreasonable maximum near the asymptotic scale, i.e., the Landau pole problem in this energy range will make it difficult to obtain a convincing prediction of the pQCD. To redefine the infrared behavior of  $\alpha_s$  within the small energy region, and achieve reliable theoretical predictions, non-perturbative methods are typically employed to capture the intricate physics occurring in the low energy region. These methods include some phenomenological low-energy models, lattice QCD, and Dyson-Schwinger equations (DSE) [44].

For the EJSR to be addressed in this paper, low-energy models are adequate to describe the physics in these energy ranges and yield highly accurate theoretical predictions. Therefore, in our investigation of the running behavior of  $\alpha_s$  at low energies, we primarily utilize low-energy model methods to enhance the precision of perturbative theoretical predictions. In the literature, numerous low-energy models for  $\alpha_s$  have been proposed [45–54]. In this paper, we adopt the analytical perturbation theory (APT) model [48] as the preferred framework for redefining the infrared behavior of  $\alpha_s$  in a way that ensures clarity and precision throughout our analysis.

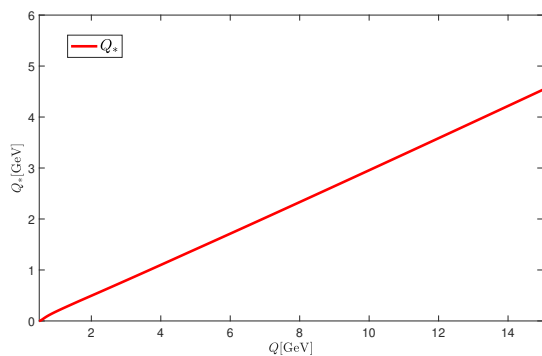


FIG. 1: The variation of  $Q_*$  changes with energy scale  $Q$ .

The APT model, analogous to the analysis of the general expression of effective charge  $\alpha_s$  in QED, employs the perturbative analytical expression of the spectral function to address the Landau pole issue. Based on the expression of the one-loop  $\alpha_s$ , its corresponding spectral

function can be briefly expressed as:

$$\rho(\delta) = \frac{\pi\beta_0^{-1}}{(\ln \frac{\delta}{\Lambda^2})^2 + \pi^2}. \quad (10)$$

The analytic running coupling is

$$\alpha_{an}(Q) = \frac{1}{\pi} \int_0^\infty \frac{\rho(\delta)}{\delta + Q^2}. \quad (11)$$

After reconstruction, the space-like domain of  $\alpha_s$  effectively eliminates all non-physical singularities, and the integration of spectral functions does not require additional subtraction. Based on Eq.10 and Eq.11, the effective coupling of APT model is formulated as follows:

$$\alpha_s^{\text{APT}}(Q) = \frac{\pi}{\beta_0} \left( \frac{1}{\ln k} + \frac{1}{1-k} \right), \quad (12)$$

where  $k = Q^2/\Lambda^2$ . Furthermore, it is worth mentioning that  $\alpha_s^{\text{APT}}(Q)$  does not incorporate any modified parameters; instead, it reconstructs the expression. The scale  $\Lambda$  can be reformulated in the following manner:

$$\Lambda^2 = Q^2 e^{-\phi(\frac{\beta_0 \alpha_s(Q)}{\pi})}, \quad (13)$$

and  $\phi(z)$  satisfies the evolution equation

$$\frac{1}{1 - e^{\phi(z)}} + \frac{1}{\phi(z)} = z. \quad (14)$$

By utilizing the value of  $\alpha_s(M_Z) = 0.1179 \pm 0.0009$  [55], which leads to  $\Lambda|_{n_f=3} = 0.339_{-0.013}^{+0.014}$  GeV,  $\Lambda|_{n_f=4} = 0.290 \pm 0.013$  GeV,  $\Lambda|_{n_f=5} = 0.207_{-0.010}^{+0.011}$  GeV.

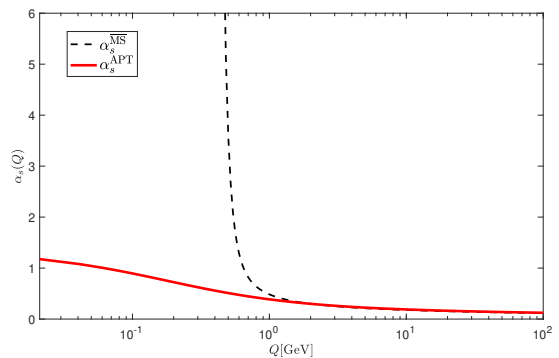


FIG. 2: The strong coupling  $\alpha_s(Q)$  versus the energy scale  $Q$ . The red line represents the APT low energy model, while the 3-loop running behavior of the  $\alpha_s$  under the  $\overline{\text{MS}}$ -scheme is depicted as a black dashed line.

Fig.2 depicts the varying behavior of  $\alpha_s$  under different scales. The red line represents the APT model, whereas the black dashed line denotes the solution obtained from RGE of Eq.2. A smooth transition of  $\alpha_s$  between the low and high-energy regions is achieved by implementing the matching scheme proposed in Ref.[56], i.e., the transition scale for  $\alpha_s$  is definitively set at  $Q_0 \approx 2.062$  GeV by enforcing the condition that the first derivatives of  $\alpha_s$  coincide at the intersection point of the two distinct energy regions.

## B. Perturbative contributions to the EJSR up to N<sup>3</sup>LO

Table I shows the coefficient convergence of the EJSR up to N<sup>3</sup>LO, obtained by both the conventional (Conv.) method and the PMC approach, across a variety of typical scales. When the renormalization scale is set to  $\mu_r = Q$ , both the conventional and PMC approaches exhibit satisfactory coefficient convergence. However, when taking into account the impact of variations in the renormalization scale on conventional calculations, i.e.,  $\mu_r \in [Q/2, 2Q]$ , the coefficient convergence is notably diminished. The convergence of the EJSR exhibits significant fluctuations under the conventional method, e.g. the conventional coefficient convergence under  $Q = 4$  GeV is  $-1.61\%^{+15.76\%}_{-1.28\%}$ .

Q	4 GeV	6 GeV	10 GeV
Conv.	$-1.61\%^{+15.76\%}_{-1.28\%}$	$-0.57\%^{+3.08\%}_{-0.80\%}$	$-0.33\%^{+1.53\%}_{-0.54\%}$
PMC	8.41%	2.45%	1.13%

TABLE I: The N<sup>3</sup>LO coefficient convergence of the EJSR for several typical scales under the conventional and PMC approach, respectively. The upper and lower errors of the conventional results stem from  $\mu_r \in [Q/2, 2Q]$ .

Fig.3 compares the EJSR obtained through both the PMC and conventional approaches with experimental results. In particular, the dotted red line stands for the central value of EJSR obtained by using the PMC approach, where the pale yellow error band comes from  $\Delta\alpha_s(M_Z) = \pm 0.0009$ . Whereas, the black solid line represents the EJSR under the conventional method, while the light blue error area arises from inaccuracies resulting from changes in the renormalization scale  $\mu_r \in [Q/2, 2Q]$  and  $\Delta\alpha_s(M_Z) = \pm 0.0009$ . The colorful error bars represent the experimental and fitting results outcomes reported in Refs.[57, 58]. The PMC method effectively eliminates the uncertainty associated with the renormalization scale that remains in conventional EJSR calculations, leading to a more precise theoretical prediction of EJSR, and indicating a higher degree of agreement with experimental data.

We evaluate the fit quality using the parameter  $\chi^2/d.o.f$ , where *d.o.f* is an abbreviation for the degree of freedom. This parameter indicates the extent to which the theory predicted EJSR agrees with the experimental data [55],

$$\chi^2/d.o.f = \frac{1}{N} \sum_{j=1}^N \left[ \frac{M_1(Q_j)|_{\text{exp.}} - M_1(Q_j)|_{\text{the.}}}{\sigma_j} \right]^2, \quad (15)$$

where ‘‘exp.’’ represents the experimental value and ‘‘the.’’ refers to the central value of the theoretical prediction.  $\sigma_j$  is the error of each experimental point. From Refs.[57, 58], we determine that the number of data points  $N = 67$ . It can be observed that by uti-

lizing the PMC to enhance the perturbative contribution, a more accurate prediction can be obtained, e.g., when applied with the PMC, yields a significantly smaller  $\chi^2/d.o.f|_{\text{PMC}} = 14.976$  compared to the conventional method  $\chi^2/d.o.f|_{\text{Conv.}} = 3.297 \times 10^9$ .

We further compared the goodness of fit using the Bayes factor  $\text{BF}_{10}$ , it can be written as

$$\text{BF}_{10} = \frac{p(\text{data}|\text{H}_1)}{p(\text{data}|\text{H}_0)}, \quad (16)$$

where the  $\text{H}_1$  represents the experimental measurements of EJSR and  $\text{H}_0$  represents the theoretical predictions of EJSR. The  $\text{BF}_{10}$  is the ratio of the marginal likelihood of  $\text{H}_1$  to that of  $\text{H}_0$ , representing the relative probabilities of the observed data under each hypothesis. A large  $\text{BF}_{10}$ -value indicates stronger evidence for the experiment and a large difference appearing in the experiment data and theoretical predictions. Again, the PMC gives a smaller  $\text{BF}_{10}|\_{\text{PMC}} = 3.055$  than  $\text{BF}_{10}|\_{\text{Conv.}} = 1.13 \times 10^4$ . We also give the Rhat value i.e., Gelman-Rubin Diagnostic Statistic to assess whether the model has converged. If Rhat is close to 1, it indicates that the sampling processes of all chains are consistent, meaning the chains have converged to the posterior distribution. Under the PMC approach, we get  $\text{Rhat} = 1.014$ . The above data further demonstrate that the PMC prediction for the EJSR has a higher goodness of fit with the experimental results.

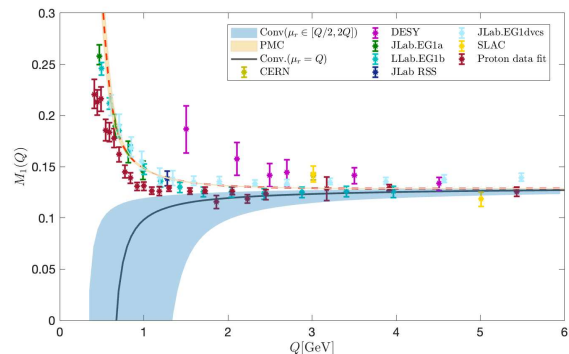


FIG. 3: The EJSR was obtained by using both the PMC and conventional approaches. The error in PMC comes from  $\Delta\alpha_s(M_Z) = \pm 0.0009$ , while in the conventional results comes from the uncertainty of  $\mu_r \in [Q/2, 2Q]$  and  $\Delta\alpha_s(M_Z) = \pm 0.0009$ .

The APT low-energy model is employed to address the infrared divergence behavior of  $\alpha_s$ . For comparison, we also display the EJSR predictions of several other low-energy models [47–49, 53, 54] proposed previously in Fig.4. This allows for a comprehensive examination of the EJSR predictions across different low-energy models.



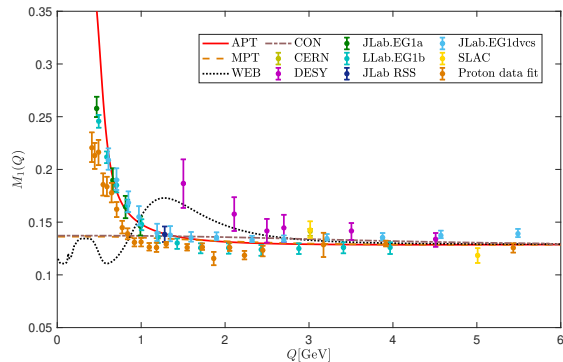


FIG. 4: The EJSR obtained by APT, CON, MPT, WEB low energy modes [47–49, 53, 54].

### C. Predictions of $\Delta\Sigma$ by Deep Learning

More importantly, the PMC conformal series, which is independent of the renormalization scale, enables us to accurately determine the value of the quark spin contribution to the nucleon spin  $\Delta\Sigma$ . Assuming only three flavors contribute to the nucleon spin, i.e.,  $n_f = 3$ , the first moment can be expressed through the proton matrix elements of the axial vector currents. Subsequently,  $\Delta\Sigma$  can be derived from the moments  $M_1(Q, \mu_r)$ . In the Quark-Parton Model (QPM), the quantity  $\Delta\Sigma$  is equivalent to the axial coupling  $a_0(Q)$ . However, within the QCD, the  $U(1)$  anomaly introduces an additional gluon contribution to  $a_0(Q)$  [1, 59], which leads to  $\Delta\Sigma$  reliant on the chosen factorization scheme. Assuming no higher-twist contribution in the Adler-Bardeen (AB) [60] factorization scheme, the relationship between  $\Delta\Sigma$  and  $a_0(Q)$  is [61]

$$a_0(Q) = \Delta\Sigma - n_f \frac{\alpha_s(Q)}{2\pi} \Delta g(Q), \quad (17)$$

where  $\Delta g$  represents the gluon contribution. It needs to be stressed that the value of  $\Delta g$  significantly influences  $\Delta\Sigma$ . However, it is crucial to acknowledge that  $\Delta g$  remains considerable uncertainties, and the existing data provides only a limited constraint on its determination. Resolving this issue is a key goal of Electron-Ion Colliders (EICs) [62, 63]. For the ensuing discussions, we adopt the values provided in Ref.[64] for subsequent numerical analysis, i.e.,  $\Delta g = 0.684$ .

We employ deep learning (DL) to simulate the value of the moments  $M_1(Q, \mu_r)$  at an arbitrary scale  $Q$ . Specifically, we use the sequential function to build a fully connected neural network. The model incorporates two hidden layers, each followed by a hyperbolic tangent (Tanh) activation function. The first hidden layer consists of 20 neurons, while the second hidden layer comprises 10 neurons. The data is divided into an 80% training set and a 20% validation set, with a maximum of 10000 training epochs. Meanwhile, to prevent overfitting, we set the

LossFunction as an indicator to evaluate model performance.

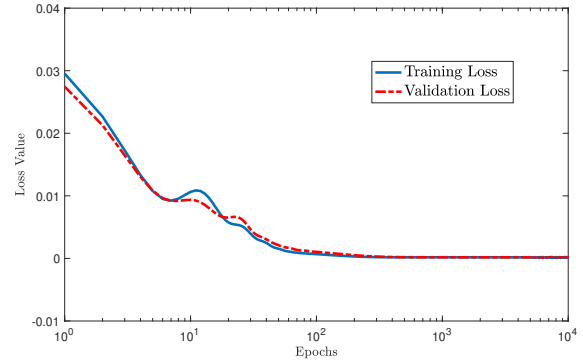


FIG. 5: The evolution of the loss function during the training epochs.

Then, we utilize the loss function and the determination coefficient (R-squared,  $R^2$ ) to assess the effectiveness of the learning quantitatively. Where the determination coefficient can be defined as

$$R^2 = 1 - \frac{\sum_{i=1}^N (y_i - \hat{y}_i)^2}{\sum_{i=1}^N (y_i - \bar{y}_i)^2}, \quad (18)$$

where  $N = 67$  denotes the number of events in the test data set, and  $y_i$  and  $\hat{y}_i$  represent the true and predicted values of the target variable, respectively. Additionally,  $\bar{y}_i$  represents the average of all test data samples. The determination coefficient  $R^2$  typically ranges from 0 to 1, with a value closer to 1 indicating superior fitting performance. In our case, we obtained an  $R^2 = 0.9237$ , which demonstrates good fitting performance.

While the  $R^2$  coefficient is a crucial indicator, a more exhaustive comprehensive understanding requires a combination of the  $R^2$  and other statistical measures. To this end, the performance of the study was further quantified using the Mean Squared Error (MSE), as illustrated in Fig.5. MSE is a loss function commonly used in regression problems (approximating continuous value function), which calculates the average of the square of the difference between the predicted value and the actual value. The equation of MSE can be expressed as:

$$\text{MSE} = \frac{1}{N} \sum_{i=1}^N (y_i - \hat{y}_i)^2. \quad (19)$$

The fluctuations in the loss function values of both the training and validation sets serve as a valuable metric for understanding the efficacy of our model training process. A smaller loss function value in the training set signifies that the model predictions increasingly align with the actual outcomes in the training data. Similarly, a decrease in the loss function value of the validation set indicates

an enhanced performance of the model when confronted with new, unseen data.

As shown in Fig.5, during the initial stages of training, we observe a decrease in the loss function value of the training set, indicating that the model is effectively learning and extracting valuable information from the training data. This progress brings its predictions progressively closer to the actual results. At the same time, a reduction in the loss function value of the validation set suggests an enhancement in the model generalization ability. The results signify that not only is the model demonstrating proficiency in managing the training data, but it is also enhancing its ability to analyze unseen data. Furthermore, the loss function values of the training and the validation are equivalent, it typically denotes an absence of overfitting in the model. Lastly, a consistent downward trend in the loss function values of both the training and validation sets, culminating in a value close to zero, which further indicates effective learning.

Based on the DL, we can get the value of  $\Delta\Sigma$  change with scale  $Q$ , as shown in Fig.6. It can be found in our analysis that with the increase of  $Q$ , the value of  $\Delta\Sigma$  tends to be stable, i.e.  $\Delta\Sigma \approx 0.23_{-0.06}^{+0.02}$ , where the error comes from the uncertainty of the experiment. This is consistent with the result obtained from a global fit of the Parton Distribution Functions (PDFs), which approximates around  $\Delta\Sigma = 0.24 \pm 0.07$  [65] see review [66] for more details. However, there are still discrepancies when compared with the extracted from the neutron  $\Delta\Sigma^{(n)} = 0.35 \pm 0.08$  [67].

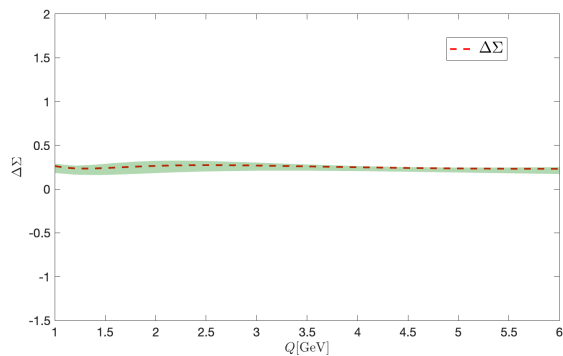


FIG. 6: The  $\Delta\Sigma$  various with  $Q$ .

## IV. SUMMARY

As a summary, in this paper, we have employed the PMC single-scale approach to address the pQCD calculable contribution to the EJSR with an accuracy up to  $N^3LO$ . Under the conventional approach, the accuracy of the EJSR is predominantly influenced by the choice of the renormalization scale. By adopting the PMC approach, we can eliminate the ambiguities associated with the conventional renormalization scale, thereby the net theoretical uncertainty is significantly reduced. Consequently, a more precise pQCD approximant for the EJSR can be obtained, as illustrated in Fig.3. The resultant PMC EJSR aligns more closely with previous experimental data. Furthermore, we also have utilized the DL method to estimate the value of  $\Delta\Sigma$ . The results show that as the scale  $Q$  increases, the  $\Delta\Sigma$  value stabilizes, culminating in an estimation of  $\Delta\Sigma \approx 0.23_{-0.06}^{+0.02}$ , where the error stems from the experimental uncertainty. This result aligns well with the global fitting outcome, which reported  $\Delta\Sigma = 0.24 \pm 0.07$ , validating the efficacy of our approach.

## V. ACKNOWLEDGMENTS

This work was supported by the Natural Science Foundation of China under Grant No.12305091, the Natural Science Foundation of Sichuan Province under Grant No.2024NSFSC1367, and the Research Fund for the Doctoral Program of the Southwest University of Science and Technology under Contract No.24zx7117 and No.23zx7122.

- 
- [1] G. Altarelli and G. G. Ross, “The Anomalous Gluon Contribution to Polarized Leptonproduction,” *Phys. Lett. B* **212**, 391-396 (1988).
  - [2] A. V. Efremov, J. Soffer and O. V. Teryaev, “Spin Structure of Nucleon and the Axial Anomaly,” *Nucl. Phys. B* **346**, 97-114 (1990).
  - [3] J. R. Ellis and M. Karliner, “Analysis of data on polarized lepton - nucleon scattering,” *Phys. Lett. B* **313**, 131-140 (1993).
  - [4] F. E. Close and R. G. Roberts, “Consistent analysis of the spin content of the nucleon,” *Phys. Lett. B* **316**, 165-171 (1993).
  - [5] G. Altarelli, P. Nason and G. Ridolfi, “On the  $Q^{*2}$  dependence of the measured polarized structure functions,” *Phys. Lett. B* **320**, 152-158 (1994) [erratum: *Phys. Lett. B* **325**, 538 (1994)].
  - [6] J. R. Ellis and R. L. Jaffe, “A Sum Rule for Deep Inelastic Electroproduction from Polarized Protons,” *Phys.*

- Rev. D **9**, 1444 (1974) [erratum: Phys. Rev. D **10**, 1669 (1974)].
- [7] A. Deur, S. J. Brodsky and G. F. De Tera mond, “The Spin Structure of the Nucleon,” doi:10.1088/1361-6633/ab0b8f [arXiv:1807.05250 [hep-ph]].
- [8] J. D. Bjorken, “Applications of the Chiral  $U(6) \times (6)$  Algebra of Current Densities,” Phys. Rev. **148**, 1467-1478 (1966).
- [9] J. Kodaira, S. Matsuda, K. Sasaki and T. Uematsu, “QCD Higher Order Effects in Spin Dependent Deep Inelastic Electroproduction,” Nucl. Phys. B **159**, 99-124 (1979).
- [10] S. G. Gorishnii and S. A. Larin, “QCD Corrections to the Parton Model Rules for Structure Functions of Deep Inelastic Scattering,” Phys. Lett. B **172**, 109-112 (1986).
- [11] S. A. Larin and J. A. M. Vermaseren, “The  $\alpha_s^3$  corrections to the Bjorken sum rule for polarized electroproduction and to the Gross-Llewellyn Smith sum rule,” Phys. Lett. B **259**, 345-352 (1991).
- [12] V. M. Braun and A. V. Kolesnichenko, “POWER CORRECTIONS TO BJORKEN AND GROSS-LLEWELLYN SMITH SUM RULES IN QCD,” Nucl. Phys. B **283**, 723-748 (1987).
- [13] I. I. Balitsky, V. M. Braun and A. V. Kolesnichenko, “Power corrections  $1/Q^{*2}$  to parton sum rules for deep inelastic scattering from polarized targets,” Phys. Lett. B **242**, 245-250 (1990) [erratum: Phys. Lett. B **318**, 648 (1993)].
- [14] Q. Yu, X. G. Wu, H. Zhou and X. D. Huang, “A novel determination of non-perturbative contributions to Bjorken sum rule,” Eur. Phys. J. C **81**, 690 (2021).
- [15] A. L. Kataev, “The Ellis-Jaffe sum rule: The Estimates of the next to next-to-leading order QCD corrections,” Phys. Rev. D **50**, R5469-R5472 (1994).
- [16] S. A. Larin, T. van Ritbergen and J. A. M. Vermaseren, “The  $\alpha_s^3$  approximation of quantum chromodynamics to the Ellis-Jaffe sum rule,” Phys. Lett. B **404**, 153-160 (1997).
- [17] A. H. Hoang, A. Jain, I. Scimemi and I. W. Stewart, “Revolution: Improving perturbative QCD,” Phys. Rev. D **82**, 011501 (2010).
- [18] X. G. Wu, S. J. Brodsky and M. Mojaza, “The Renormalization Scale-Setting Problem in QCD,” Prog. Part. Nucl. Phys. **72**, 44-98 (2013).
- [19] X. G. Wu, J. M. Shen, B. L. Du, X. D. Huang, S. Q. Wang and S. J. Brodsky, “The QCD renormalization group equation and the elimination of fixed-order scheme-and-scale ambiguities using the principle of maximum conformality,” Prog. Part. Nucl. Phys. **108**, 103706 (2019).
- [20] C. G. Callan, Jr., “Broken scale invariance in scalar field theory,” Phys. Rev. D **2**, 1541-1547 (1970).
- [21] K. Symanzik, “Small distance behavior in field theory and power counting,” Commun. Math. Phys. **18**, 227-246 (1970).
- [22] A. Peterman, “Renormalization Group and the Deep Structure of the Proton,” Phys. Rept. **53**, 157 (1979).
- [23] X. G. Wu, Y. Ma, S. Q. Wang, H. B. Fu, H. H. Ma, S. J. Brodsky and M. Mojaza, “Renormalization Group Invariance and Optimal QCD Renormalization Scale-Setting,” Rept. Prog. Phys. **78**, 126201 (2015).
- [24] M. Czakon, “The Four-loop QCD beta-function and anomalous dimensions,” Nucl. Phys. B **710**, 485-498 (2005).
- [25] P. A. Baikov, K. G. Chetyrkin and J. H. Kühn, “Five-Loop Running of the QCD coupling constant,” Phys. Rev. Lett. **118**, 082002 (2017).
- [26] T. Luthe, A. Maier, P. Marquard and Y. Schröder, “Towards the five-loop Beta function for a general gauge group,” JHEP **07**, 127 (2016).
- [27] F. Herzog, B. Ruijl, T. Ueda, J. A. M. Vermaseren and A. Vogt, “The five-loop beta function of Yang-Mills theory with fermions,” JHEP **02**, 090 (2017).
- [28] K. G. Chetyrkin, G. Falcioni, F. Herzog and J. A. M. Vermaseren, “Five-loop renormalisation of QCD in covariant gauges,” JHEP **10**, 179 (2017).
- [29] S. J. Brodsky and X. G. Wu, “Self-Consistency Requirements of the Renormalization Group for Setting the Renormalization Scale,” Phys. Rev. D **86**, 054018 (2012).
- [30] S. J. Brodsky and X. G. Wu, “Eliminating the Renormalization Scale Ambiguity for Top-Pair Production Using the Principle of Maximum Conformality,” Phys. Rev. Lett. **109**, 042002 (2012).
- [31] S. J. Brodsky and X. G. Wu, “Scale Setting Using the Extended Renormalization Group and the Principle of Maximum Conformality: the QCD Coupling Constant at Four Loops,” Phys. Rev. D **85**, 034038 (2012) [erratum: Phys. Rev. D **86**, 079903 (2012)].
- [32] S. J. Brodsky and L. Di Giustino, “Setting the Renormalization Scale in QCD: The Principle of Maximum Conformality,” Phys. Rev. D **86**, 085026 (2012).
- [33] M. Mojaza, S. J. Brodsky and X. G. Wu, “Systematic All-Orders Method to Eliminate Renormalization-Scale and Scheme Ambiguities in Perturbative QCD,” Phys. Rev. Lett. **110**, 192001 (2013).
- [34] S. J. Brodsky, M. Mojaza and X. G. Wu, “Systematic Scale-Setting to All Orders: The Principle of Maximum Conformality and Commensurate Scale Relations,” Phys. Rev. D **89**, 014027 (2014).
- [35] H. Zhou, J. Yan, Q. Yu and X. G. Wu, “Updated determination of the pion-photon transition form factor,” Phys. Rev. D **108**, 074020 (2023).
- [36] J. M. Shen, X. G. Wu, B. L. Du and S. J. Brodsky, “Novel All-Orders Single-Scale Approach to QCD Renormalization Scale-Setting,” Phys. Rev. D **95**, 094006 (2017).
- [37] X. G. Wu, J. M. Shen, B. L. Du and S. J. Brodsky, “Novel demonstration of the renormalization group invariance of the fixed-order predictions using the principle of maximum conformality and the  $C$ -scheme coupling,” Phys. Rev. D **97**, 094030 (2018).
- [38] E. C. G. Stueckelberg de Breidenbach and A. Petermann, “Normalization of constants in the quanta theory,” Helv. Phys. Acta **26**, 499-520 (1953).
- [39] M. Gell-Mann and F. E. Low, “Quantum electrodynamics at small distances,” Phys. Rev. **95**, 1300-1312 (1954).
- [40] H. Y. Bi, X. G. Wu, Y. Ma, H. H. Ma, S. J. Brodsky and M. Mojaza, “Degeneracy Relations in QCD and the Equivalence of Two Systematic All-Orders Methods for Setting the Renormalization Scale,” Phys. Lett. B **748**, 13-18 (2015).
- [41] J. Kodaira, “QCD Higher Order Effects in Polarized Electroproduction: Flavor Singlet Coefficient Functions,” Nucl. Phys. B **165**, 129-140 (1980).
- [42] S. A. Larin, “The Next-to-leading QCD approximation to the Ellis-Jaffe sum rule,” Phys. Lett. B **334**, 192-198 (1994).
- [43] M. Tanabashi *et al.* [Particle Data Group], “Review of Particle Physics,” Phys. Rev. D **98**, 030001 (2018).
- [44] Q. Yu, H. Zhou, X. D. Huang, J. M. Shen and X. G. Wu,

- “Novel and Self-Consistency Analysis of the QCD Running Coupling  $\alpha_s(Q)$  in Both the Perturbative and Non-perturbative Domains,” *Chin. Phys. Lett.* **39**, 071201 (2022).
- [45] J. M. Cornwall, “Dynamical Mass Generation in Continuum QCD,” *Phys. Rev. D* **26**, 1453 (1982).
- [46] S. Godfrey and N. Isgur, “Mesons in a Relativized Quark Model with Chromodynamics,” *Phys. Rev. D* **32**, 189-231 (1985).
- [47] F. Halzen, G. I. Krein and A. A. Natale, “Relating the QCD pomeron to an effective gluon mass,” *Phys. Rev. D* **47**, 295-298 (1993).
- [48] D. V. Shirkov and I. L. Solovtsov, “Analytic model for the QCD running coupling with universal  $\alpha_s(0)$  value,” *Phys. Rev. Lett.* **79**, 1209-1212 (1997).
- [49] B. R. Webber, “QCD power corrections from a simple model for the running coupling,” *JHEP* **10**, 012 (1998).
- [50] A. M. Badalian and D. S. Kuzmenko, “Freezing of QCD coupling  $\alpha_s$  affects the short distance static potential,” *Phys. Rev. D* **65**, 016004 (2001).
- [51] S. J. Brodsky, G. F. de Teramond and A. Deur, “Nonperturbative QCD Coupling and its  $\beta$ -function from Light-Front Holography,” *Phys. Rev. D* **81**, 096010 (2010).
- [52] D. V. Shirkov, “Nonpower expansions for QCD observables at low energies,” *Nucl. Phys. B Proc. Suppl.* **152**, 51-56 (2006).
- [53] D. V. Shirkov, “The Unitary mechanism of infrared freezing in QCD with massive gluons,” *Phys. Atom. Nucl.* **62**, 1928-1931 (1999).
- [54] D. V. Shirkov, “Massive’ Perturbative QCD, regular in the IR limit,” *Phys. Part. Nucl. Lett.* **10**, 186-192 (2013).
- [55] R. L. Workman *et al.* [Particle Data Group], “Review of Particle Physics,” *PTEP* **2022**, 083C01 (2022).
- [56] A. Deur, S. J. Brodsky and G. F. de Teramond, “Connecting the Hadron Mass Scale to the Fundamental Mass Scale of Quantum Chromodynamics,” *Phys. Lett. B* **750**, 528-532 (2015).
- [57] M. Osipenko, S. Simula, W. Melnitchouk, P. E. Bosted, V. Burkert, E. Christy, K. Griffioen, C. Keppel, S. E. Kuhn and G. Ricco, “Global analysis of data on the proton structure function  $g(1)$  and extraction of its moments,” *Phys. Rev. D* **71**, 054007 (2005).
- [58] R. Fersch *et al.* [CLAS], “Determination of the Proton Spin Structure Functions for  $0.05 < Q^2 < 5\text{GeV}^2$  using CLAS,” *Phys. Rev. C* **96**, 065208 (2017).
- [59] R. D. Carlitz, J. C. Collins and A. H. Mueller, “The Role of the Axial Anomaly in Measuring Spin Dependent Parton Distributions,” *Phys. Lett. B* **214**, 229-236 (1988).
- [60] S. L. Adler and W. A. Bardeen, “Absence of higher order corrections in the anomalous axial vector divergence equation,” *Phys. Rev.* **182**, 1517-1536 (1969).
- [61] R. D. Ball, S. Forte and G. Ridolfi, “Scale dependence and small-x behavior of polarized parton distributions,” *Nucl. Phys. B* **444**, 287-309 (1995) [erratum: *Nucl. Phys. B* **449**, 680-680 (1995)].
- [62] D. P. Anderle, V. Bertone, X. Cao, L. Chang, N. Chang, G. Chen, X. Chen, Z. Chen, Z. Cui and L. Dai, *et al.* “Electron-ion collider in China,” *Front. Phys. (Beijing)* **16**, 64701 (2021).
- [63] R. Abdul Khalek, A. Accardi, J. Adam, D. Adamiak, W. Akers, M. Albaladejo, A. Al-bataineh, M. G. Alexeev, F. Ameli and P. Antonioli, *et al.* “Science Requirements and Detector Concepts for the Electron-Ion Collider: EIC Yellow Report,” *Nucl. Phys. A* **1026**, 122447 (2022).
- [64] M. Gluck, E. Reya, M. Stratmann and W. Vogelsang, “Models for the polarized parton distributions of the nucleon,” *Phys. Rev. D* **63**, 094005 (2001).
- [65] M. Hirai *et al.* [Asymmetry Analysis], “Determination of gluon polarization from deep inelastic scattering and collider data,” *Nucl. Phys. B* **813**, 106-122 (2009).
- [66] C. A. Aidala, S. D. Bass, D. Hasch and G. K. Mallot, “The Spin Structure of the Nucleon,” *Rev. Mod. Phys.* **85**, 655-691 (2013).
- [67] J. P. Chen, A. Deur and Z. E. Meziani, “Sum rules and moments of the nucleon spin structure functions,” *Mod. Phys. Lett. A* **20**, 2745-2766 (2005).